New crystal structure maps for intermetallic compounds

1997 J. Phys.: Condens. Matter 9 8011

(http://iopscience.iop.org/0953-8984/9/38/008)

J. Phys.: Condens. Matter **9** (1997) 8011–8030. Printed in the UK PII: S0953-8984(97)84318-4

New crystal structure maps for intermetallic compounds

Yoshihisa Harada†, Masahiko Morinaga†, Jun-ichi Saito‡‖ and Yasuharu Takagi§¶

† Department of Materials Science and Engineering, Graduate School of Engineering, Nagoya University, Furo-cho, Chikusa-ku, Nagoya, Aichi, 464-01, Japan

‡ Department of Production Systems Engineering, Toyohashi University of Technology, Tempaku-cho, Toyohashi, Aichi, 441, Japan

§ Department of Production Systems Engineering, Toyohashi University of Technology, Tempaku-cho, Toyohashi, Aichi, 441, Japan

Received 20 May 1997

Abstract. New crystal structure maps have been proposed on the basis of the DV-X_α molecular orbital calculations of electronic structures. Two electronic parameters have been introduced and employed as new parameters for the classification of crystal structures. One is the bond order and the other is the d-orbital energy level of elements. Both of them change following the position of elements in the periodic table. With these parameters crystal structure maps have been constructed for aluminides, silicides, and some transition-metal-based compounds. There is a clear separation of the crystal structures on the maps. These maps are found to be applicable to the prediction of crystal structures not only for binary compounds but also for ternary compounds. The possibilities of structural modification of Nb_3Al and Al_3Ti by alloying are also discussed with the aid of these maps.

1. Introduction

Crystal structures of intermetallic compounds change greatly with the combination of constituent elements in them [1]. This is in contrast with metals and alloys, having only a few crystal structures. The physical and chemical properties of intermetallic compounds depend strongly on the crystal structures, so many attempts have been made to improve their properties through structural modification, for example, by adding ternary elements into mother compounds [2, 3]. It may be said that the prediction of crystal structures is indeed a first step to the design of intermetallic compounds.

A pioneering work for the structural separation of compounds was performed using the average number of valence electrons per atom (e/a) by Hume-Rothery in 1934, and these compounds are sometimes called electron compounds. Since then, many investigators have attempted to put in order crystal structural data on two- or three-dimensional structure maps employing a variety of parameters such as the electronegativity, the pseudopotential radius [4–7], and the Mendeleev number [8, 9]. However, despite great effort to predict the crystal structures of the compounds, there are still some difficulties in these approaches, as explained later. The total-energy calculation has also been used for treating the structural

‖ Present address: Oarai Engineering Centre, Power Reactor and Nuclear Fuel Development Corporation, 4002 Narita, Oarai-machi, Higashi-Ibaraki, Ibaraki, 311-13, Japan.

¶ Present address: Semiconductor Devices Division, Japanese Patent Office, 4-3 Kasumigaseki 3-chome, Chiyoda-ku, Tokyo, 100, Japan.

0953-8984/97/388011+20$19.50

stability of compounds, but the structural map is still desired in view of the efficient design of intermetallic compounds.

In this paper, two electronic parameters which represent the nature of the chemical bond between atoms in intermetallic compounds, have been calculated by the DV-X_α molecular orbital method. Employing these electronic parameters, new crystal structure maps have been proposed for aluminides, silicides, and some transition-metal-based compounds. As a practical application, the possibility of structural modification of a few aluminides by alloying will be discussed with the aid of these maps.

2. Calculation method

2.1. The DV-X_α molecular orbital method

The DV-X_α molecular orbital method is based on the Hartree–Fock–Slater approximation, and it provides fairly accurate electronic structures even for a large size of atom clusters [10–13].

In this calculation, an exchange–correlation interaction between electrons is given by the following Slater's X_α potential [14], V_{xc},

$$V_{xc}(r) = -3\alpha\{3/8\pi\rho(r)\}^{1/3} \tag{1}$$

where $\rho(r)$ is the local electron density. The parameter α is fixed at 0.7, an empirically appropriate value [10] and the self-consistent charge approximation is used in the calculation. The matrix elements of the Hamiltonian and the overlap integrals are calculated by a random sampling method. The molecular orbitals are constructed by a linear combination of numerically generated atomic orbitals. The atomic orbitals used in this study are 1s–3d for Al and Si, and 1s–*n*p for transition metals, M ($n = 4$ for 3d transition metals, $n = 5$ for 4d transition metals, and $n = 6$ for 5d transition metals). Further explanation of the calculation method is given elsewhere [14, 15].

2.2. The cluster model

The selection of the cluster model is most crucial in the present calculation. Generally, any crystal structure may be divided into a number of small polyhedra. However, according to mathematical models [16], there are four simple polyhedra. They are tetrahedron, octahedron, hexahedron (cube) and icosahedron. Among them the icosahedron is one of the five Platonic solids, next in simplicity to the tetrahedron and the octahedron, and this is actually observed in quasi-crystals. For crystalline solids, the other three polyhedra may be important structural units. In this study, among them an octahedral model is chosen in order to express atomic interactions as simply as possible and also to increase the applicability of the results to a variety of crystal structures of intermetallic compounds. The actual cluster model used is shown in figure 1(a). Such an octahedron is often seen in the structures of compounds. For example, as shown in figure 1(b–d), there is an octahedral structural unit, M_2X_4, in B2 (CsCl-type), $L1_0$ (CuAu-type) and $L1_2$(Cu_3Au-type) structures.

For aluminides, as shown in figure 1(a), Al is set on X, and an M_2Al_4 cluster is used in the calculation, where the M are transition metals: Sc, Ti, V, Cr, Mn, Fe, Co, Ni, Cu (3d transition metals), Y, Zr, Nb, Mo, Tc, Ru, Rh, Pd, Ag (4d transition metals), and La, Hf, Ta W, Re, Os, Ir, Pt, Au (5d transition metals). The *a*-axial length is fixed at 0.2864 nm, twice as large as the aluminium atomic radius, and the *c*-axial length is varied following the atomic radius of M so that the M atom sphere contacts with the Al atom sphere as

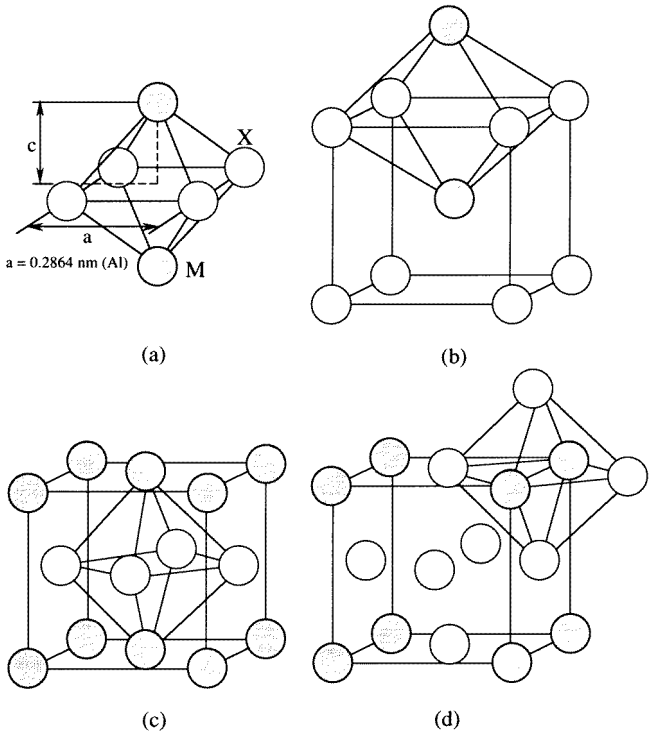

Figure 1. (a) Octahedral cluster model, M_2X_4, and typical crystal structures containing octahedral clusters, (b) B2-type, (c) $L1_0$-type and (d) $L1_2$-type structures.

if they are rigid-body spheres. For silicides, a similar cluster model, M_2Si_4, is employed except for the a-axial length of 0.2638 nm, twice as large as the silicon atomic radius. For transition-metal-based compounds, metals set on X are Ti, Fe, Ni, Nb, and Mo, and similar calculations are carried out with the M_2X_4 cluster for a variety of transition metals, M.

In order to show the validity of the results obtained by the octahedral model, further calculation is performed with a large $MoSi_2$-based cluster model containing the octahedron, tetrahedron, and hexahedron as well.

2.3. Analysis of electronic structures

The electronic structure of intermetallic compounds may be characterized by the energy level structure in a cluster [11] and also the bond order between atoms [17].

Following the Mulliken population analysis, the overlap population of electrons between atoms is obtained. The overlap population, $Q_{\nu\nu'}$, of electrons between two atoms ν and ν' is defined as

$$Q_{\nu\nu'} = \sum_i \sum_{i,j} C_{il}^{\nu} C_{jl}^{\nu'} \int \psi_i^* \psi_j \, \mathrm{d}V. \tag{2}$$

Here, ψ_i and ψ_j are the wavefunctions of the i and j orbitals of atoms ν and ν', respectively. C_{il}^{ν} and $C_{jl}^{\nu'}$ are the coefficients which show the magnitude of the linear combination of atomic orbitals in the lth molecular orbital. This $Q_{\nu\nu'}$ corresponds to the bond order (hereafter referred to as Bo). The bond order is a measure of the strength of the covalent

bond between atoms. A higher bond order means a stronger chemical bond existing between atoms. For example, when X and M atoms are both transition metals such as Mo, Nb, Ti, Fe, and Ni, d–d covalent interactions are mainly responsible for their high cohesive energies [18], so the bond order is estimated from the overlap populations between X d electrons and M d electrons. On the other hand, when X is a non-transition metal such as Al and Si, but M is a transition metal, p–d covalent interactions are probably most important, so the bond order is estimated from the overlap population between X p electrons and M d electrons. The bond order calculated in this way is used here as a new parameter to construct the structure maps of compounds.

In addition, the d-orbital energy level of transition element is determined as another new parameter. Hereafter, this is referred to as Md. This parameter is associated with two classical parameters, the electronegativity and the atomic radius of element M, as shown later. The electronegativity is concerned with the charge transfer between atoms, and hence this parameter is a sort of measure to show the ionic interaction between atoms. Also, as the Md parameter is related closely to the atomic size, the use of this parameter may guarantee the structural classification even for size-controlling compounds such as the Laves phases.

It is stressed here that both the Bo and the Md are parameters determined by the calculation of electronic structures. By recalling that every element is arranged in the periodic table according to the outer-electron configurations, it is inevitable that these electronic parameters change periodically, following the position of elements in the periodic table, as explained later. In other words, two parameters well reflect rules or information relevant to the periodic table of elements.

3. Calculation of electronic parameters

3.1. d-orbital energy level, Md

The energy level structures are shown in figure 2 for the M_2Al_4 cluster where the M are 3d transition metals. The 3d component of the M metal appears in the broad Al s, p band which extends from -8 to 4 eV as shown in figure 2. The energy of the Fermi level, E_F, is indicated by an arrow in each energy level structure.

A large fraction of the d component appears, for example, in the b_{2u} level, because of the D_{4h} symmetry of the cluster. In fact, the $2b_{2u}$ level consists of the d component to more than 90%, and some other minor components. As shown in figure 2, the height of the $2b_{2u}$ level changes monotonically with the order of elements in the periodic table, and this is supposed to be the level characteristic of M in the M_2Al_4 cluster. Also, the $3b_{2u}$ level exists in the energy range of several electron volts higher than the $2b_{2u}$ level. So, the average d-orbital energy level, Md, is calculated by taking a weighted average of the energies for the $2b_{2u}$ and $3b_{2u}$ levels using a weighting factor of the 3d component in each level. The variation of the Md level with elements, M, is shown in figure 3(a), and it is compared with the change in the atomic radius and the electronegativity of elements as shown in figure 3(b).

As explained earlier, the value of Md changes periodically with the order of elements in the periodic table. Also, it tends to increase with increasing atomic radius of the element, M [19], except for Cu, Rh, Pd, Ag, Ir, Pt, Au, all of which are elements having the d orbitals nearly filled with electrons. This correlation between the Md and the atomic radius is due simply to the weakening of the attractive Coulomb interaction operating between the d electrons and a nucleus with increasing average d-orbital radius, resulting in the higher energy of the Md level. In addition, as shown in figure 3(b), the value of Md increases with

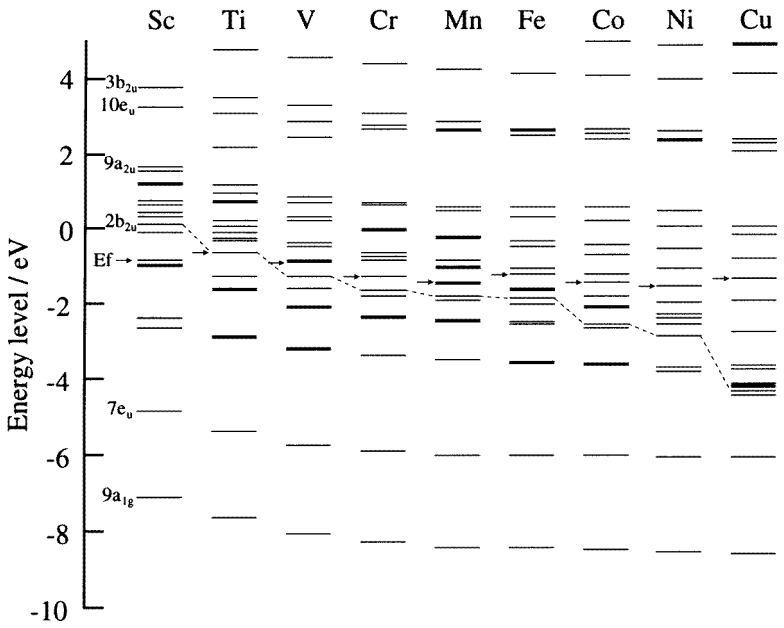

Figure 2. Energy level structures for the M_2Al_4 cluster with 3d transition metals, M.

decreasing electronegativity of the element, M [20]. This correlation is also reasonable, since it is known that the energy level obtained by the X_α method represents the electronegativity value itself [15, 17]. There is a general trend that a larger atom has a lower electronegativity value. Thus, Md is an atomic size parameter as well as a chemical parameter to represent the ionic interaction between M and X atoms through the charge transfer between those atoms.

A level other than the b_{2u} level may be selected, but other molecular levels also change in a similar way as does the b_{2u} level as shown in figure 4. This is also true for the a_{1g}, a_{2u}, e_g, and e_u levels, although they are not shown in the figure.

3.2. Bond order, Bo

As explained before, the bond order is a parameter to show the overlapping of electron clouds between atoms, and hence this is a measure of the covalent bond strength between atoms. The bond orders are calculated between M d electrons and Al 3p electrons for the M_2Al_4 cluster and between M d electrons and Si 3p electrons for the M_2Si_4 cluster. The results are shown in figure 5(a). Both the bond orders change periodically following the position of elements in the periodic table. There are peaks in the bond order curve near Cr, Mo, and W in the series of 3d, 4d, and 5d transition metals, respectively, all of which are elements in the 6A group. For comparison, the melting temperatures of MAl, M_3Al, and MAl_3 compounds are also shown in figure 5(b). There is a general trend that the melting temperature changes in a similar way as does the M–Al bond order, except for Cr, Mn, and Fe in the series of the 3d transition metals, where there is a steep drop in the melting temperatures of the compounds. Such a drop is, however, observed even in the melting temperatures of the pure 3d transition metals.

Table 1. Md and Bo values for elements, M, in M_2X_4 and $MMo_{12}Si_{18}$ clusters.

Element	M_2Al_4 cluster		M_2Si_4 cluster		M_2Ti_4 cluster		M_2Fe_4 cluster		M_2Ni_4 cluster		M_2Nb_4 cluster		M_2Mo_4 cluster		$M_1Mo_{12}Si_{18}$ cluster	
	Md	Bo(d-3p)	Md	Bo(d-3p)	Md	Bo(d-3d)	Md	Bo(d-3d)	Md	Bo(d-3d)	Md	Bo(d-4d)	Md	Bo(d-4d)	Md	Bo(d-3p)
Sc	0.802	0.731	-0.184	1.082	2.239	0.591	1.012	0.612	0.333	0.471	2.141	0.767	1.733	0.838		
Ti	0.144	1.034	-0.541	1.573	1.476	0.809	0.164	0.913	-0.825	0.640	1.138	1.101	0.758	1.138	4.524	0.642
V	-0.528	1.282	-0.581	1.684	0.989	1.086	-0.389	0.959	-0.991	0.682	0.776	1.409	0.344	1.392	3.901	0.673
Cr	-0.996	1.405	-1.131	1.719	0.385	1.189	-0.932	0.987	-1.457	0.629	0.080	1.442	-0.225	1.434	3.508	0.652
Mn	-1.225	1.274	-1.433	1.585	0.115	1.113	-1.405	0.825	-1.738	0.482	-0.342	1.340	-0.581	1.218	3.112	0.599
Fe	-1.399	1.115	-1.883	1.250	-0.293	0.969	-1.625	0.528	-2.013	0.278	-0.700	1.064	-1.099	1.020	2.853	0.481
Co	-1.646	1.044	-2.177	0.992	-0.679	0.698	-1.909	0.307	-2.278	0.112	-1.208	0.863	-1.433	0.745	2.669	0.367
Ni	-2.238	0.711	-2.883	0.665	-1.284	0.466	-2.481	0.162	-2.607	-0.041	-1.831	0.589	-1.858	0.414	2.491	0.243
Cu	-4.023	0.253	-4.379	0.256	-2.399	0.138	-3.590	-0.050	-3.820	-0.101	-2.576	0.151	-3.115	0.111		
Y	0.784	0.842	0.042	1.196	2.632	0.660	1.703	0.643	0.337	0.607	2.565	0.879	2.279	0.947		
Zr	0.000	1.222	-0.137	1.826	1.817	0.944	0.849	0.872	-0.457	0.787	1.735	1.256	1.240	1.327	5.654	0.873
Nb	-0.081	1.346	-0.250	2.027	1.325	1.240	0.005	1.100	-0.790	0.848	1.111	1.599	0.685	1.648	5.079	0.939
Mo	-0.819	1.550	-1.020	2.096	0.470	1.351	-0.692	1.067	-1.280	0.711	0.332	1.720	0.065	1.568	4.184	0.928
Tc	-1.474	1.645	-1.519	2.012	-0.062	1.339	-1.463	1.046	-1.759	0.627	-0.463	1.652	-0.713	1.511		
Ru	-2.031	1.494	-1.767	1.625	-0.612	1.079	-1.977	0.706	-2.287	0.384	-1.023	1.353	-1.486	1.304	3.577	0.654
Rh	-2.336	1.280	-2.751	1.161	-1.473	0.834	-2.653	0.455	-2.855	0.135	-1.878	1.020	-2.133	0.859		
Pd	-3.338	0.714	-4.030	0.575	-2.411	0.423	-3.231	0.024	-3.440	-0.082	-2.713	0.484	-2.870	0.358		
Ag	-6.084	0.213	-6.221	0.123	-4.505	0.054	-5.646	-0.107	-5.994	-0.101	-4.670	0.056	-5.078	0.025		
La	1.771	0.952	1.796	1.244	2.756	0.682	1.847	0.828	0.486	0.578	2.769	0.956	2.508	0.999		
Hf	0.762	1.354	-0.056	1.930	2.034	1.051	0.993	1.057	-0.273	0.838	1.953	1.326	1.467	1.408	5.530	0.985
Ta	0.055	1.432	-0.432	2.054	1.589	1.291	-0.027	1.144	-0.714	0.910	1.396	1.677	0.930	1.743	5.078	1.046
W	-0.699	1.672	-0.809	2.177	0.890	1.412	-0.484	1.135	-0.949	0.755	0.684	1.824	0.219	1.826	4.611	0.995
Re	-1.403	1.784	-1.414	2.170	0.116	1.430	-1.304	1.114	-1.583	0.604	-0.260	1.771	-0.512	1.623	3.931	0.817
Os	-1.783	1.626	-2.198	1.717	-0.563	1.158	-1.839	0.864	-2.090	0.418	-0.885	1.474	-1.350	1.438		
Ir	-2.373	1.432	-2.815	1.262	-1.455	0.919	-2.468	0.407	-2.694	0.148	-1.842	1.143	-2.086	0.971		
Pt	-3.562	0.820	-4.237	0.640	-2.719	0.582	-3.414	0.006	-3.541	-0.103	-2.993	0.706	-2.993	0.407		
Au	-6.210	0.282	-6.316	0.168	-4.557	0.080	-5.733	-0.101	-5.950	-0.138	-4.726	0.083	-5.128	0.041		
Al					1.105	0.358	-0.095	0.360	-0.740	0.291	0.937	0.479	0.566	0.488		
Si					-0.278	0.334	-1.325	0.414	-1.762	0.327	-0.408	0.473	-0.679	0.660		

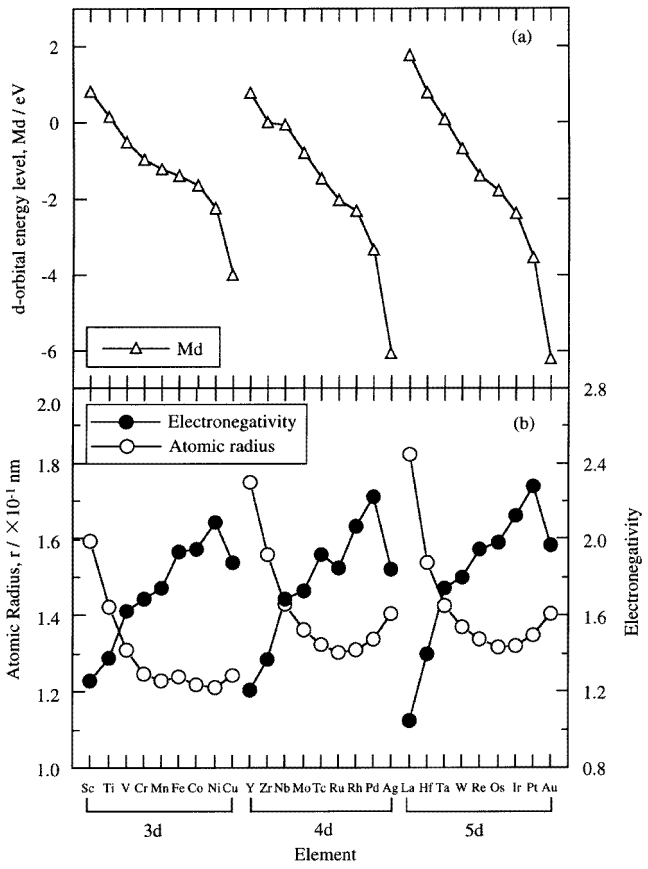

Figure 3. Changes in (a) the d-orbital energy level for the M_2Al_4 cluster, (b) the atomic radius [19] and the electronegativity [20], with elements, M.

Thus, the concept of the covalent bonding, ionic bonding, and atomic size, all of which are important factors in determining crystal structures, is involved in the two calculated parameters, the bond order, Bo, and the d-orbital energy level, Md. Furthermore, both of them change following the position of elements in the periodic table. This is very important since the crystal structures of compounds also change following the periodic table. In fact, the same or similar crystal structure appears in the same group or its neighbourhood in the periodic table. In this sense, these Bo and Md are indeed suitable parameters for constructing structure maps.

For convenience, the respective values for the Bo and the Md parameters are listed in table 1. For non-transition metals, Al and Si, the Md values could not be obtained from the calculation. In order to treat these metals in the same framework as the transition metals, they are determined empirically using a correlation between the Md value and the electronegativity of elements. Namely, the calculated Md values for various transition metals are first plotted against the values of electronegativities, and then each Md value is interpolated at the position of the electronegativity value of 1.5 for Al and 1.8 for Si [20]. The values determined in this way are also listed in table 1.

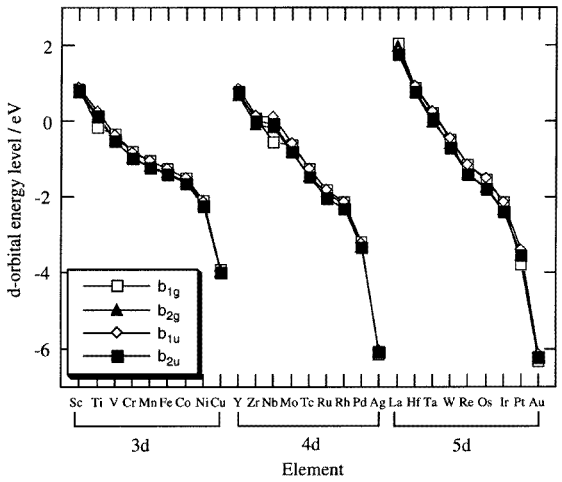

Figure 4. A comparison of the d-orbital energy level among the b_{1g}, b_{2g}, b_{1u}, and b_{2u} levels for the M_2Al_4 cluster.

4. Structure maps

4.1. Aluminides

The structure maps are constructed using the bond order (Bo) and the d-orbital energy level (Md). The examples are shown in figure 6 for aluminides, (a) MAl, (b) M_3Al, and (c) MAl_3. All these maps are drawn using the Bo and the Md values for the M_2Al_4 cluster, listed in table 1. The crystal structure data of intermetallic compounds are taken from the *Pearson's Handbook* [1]. Each crystal structure is distinguished from the others using different symbols on the map. In addition to binary compounds, ternary compounds, for example, $(M_{1-x}Y_x)Al$, Nos 1–6 shown in figure 6(a), are also located on the map, simply by taking the compositional average of the Bo and the Md parameters. Namely,

$$\mathrm{Bo} = (1-x)(\mathrm{Bo})_M + x(\mathrm{Bo})_Y \tag{3}$$

$$\mathrm{Md} = (1-x)(\mathrm{Md})_M + x(\mathrm{Md})_Y. \tag{4}$$

The crystal structures are well separated in each map. For example, for the MAl map, TiAl with the $L1_0$-type structure is located between the B33-type and the B2-type compounds on the map. PtAl and PdAl take the B20-type structure at low temperatures and the B2-type structure at high temperatures. In response to this, the B20-type region lies at the edge of the B2-type region. For the M_3Al map shown in figure 6(b), the A15-type region is located in a high-Bo region on the map. The $D0_{19}$-type region lies between the A15-type and the $L1_2$-type regions. Ternary compounds of Nos 1–19 have either the $D0_3$-type or the $L2_1$-type structure. Here, the $D0_3$- and the $L2_1$-type structures resemble each other as shown in figure 6(b-1) and (b-2), respectively, and hence their regions are nearly overlapped on the map. For the MAl_3 map shown in figure 6(c), there is the $D0_{22}$-type region near the $D0_{23}$-type region, because of the structural resemblance between them. In fact, $HfAl_3$ takes both the $D0_{22}$-type and the $D0_{23}$-type structures, varying with the temperature.

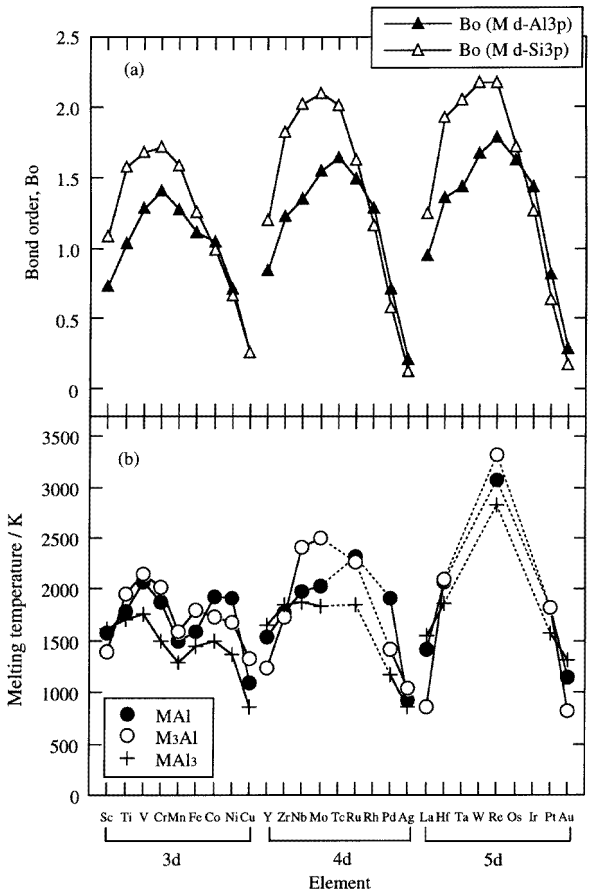

Figure 5. Changes in (a) the M–Al and the M–Si bond orders and (b) the melting temperatures of aluminides with M.

4.2. Silicides

The structure maps for silicides are shown in figure 7: (a) MSi, (b) M_3Si, and (c) MSi_2. In each map, there is a good separation of the crystal structures. For example, as shown in figure 7(c), the $C11_b$-type region of $MoSi_2$ [21] is located in a high-Bo region, and adjacent to the C40-type region on the map. This is reasonable since even for pure $MoSi_2$ the C40-type structure is found when it is rapidly quenched from the melt, even though this may be a metastable phase [22]. It is also known that if a (110) stacking fault is introduced into the $C11_b$-type structure, the crystal structure becomes identical with the C40-type structure. Also, as shown in figure 7(b), the A15-type region is close to the PTi_3 region, since both of them appear, for example, in Nb_3Si.

4.3. Transition-metal-based compounds

Furthermore, a series of structure maps is shown in figure 8 for (a) M_3Ti, (b) MNi, and (c) MNi_3, and in figure 9 for (a) MFe, (b) MNb_3, and (c) MMo. It is evident that crystal structures are clearly separated in these maps.

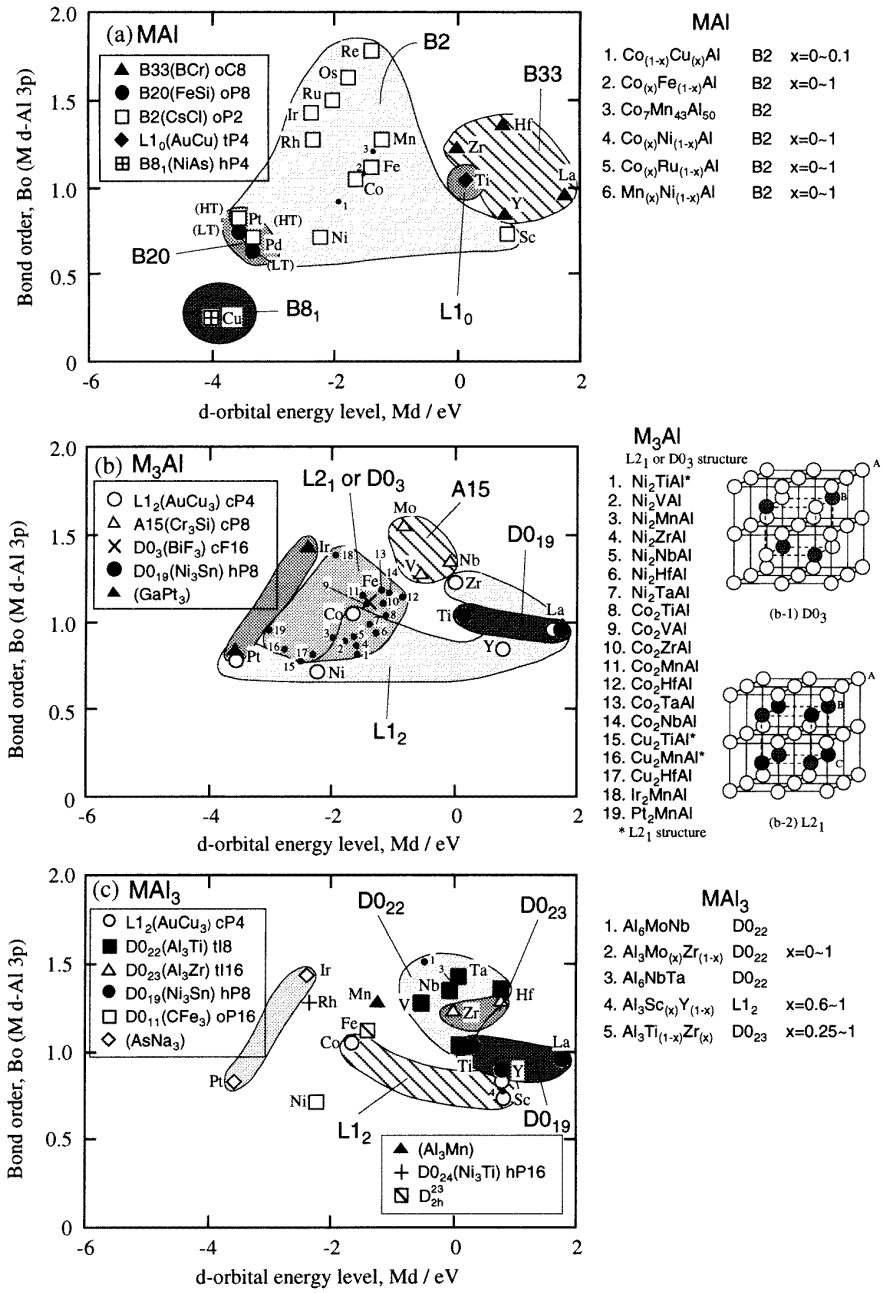

Figure 6. Structure maps for (a) MAl, (b) M_3Al, and (c) MAl_3 compounds. Crystal structures are denoted using the Structurbericht symbol or the Pearson symbol.

5. Cluster model dependence on electronic parameters

Two electronic parameters are determined using an octahedral cluster model shown in figure 1(a). However, the results may be dependent on the model employed in the

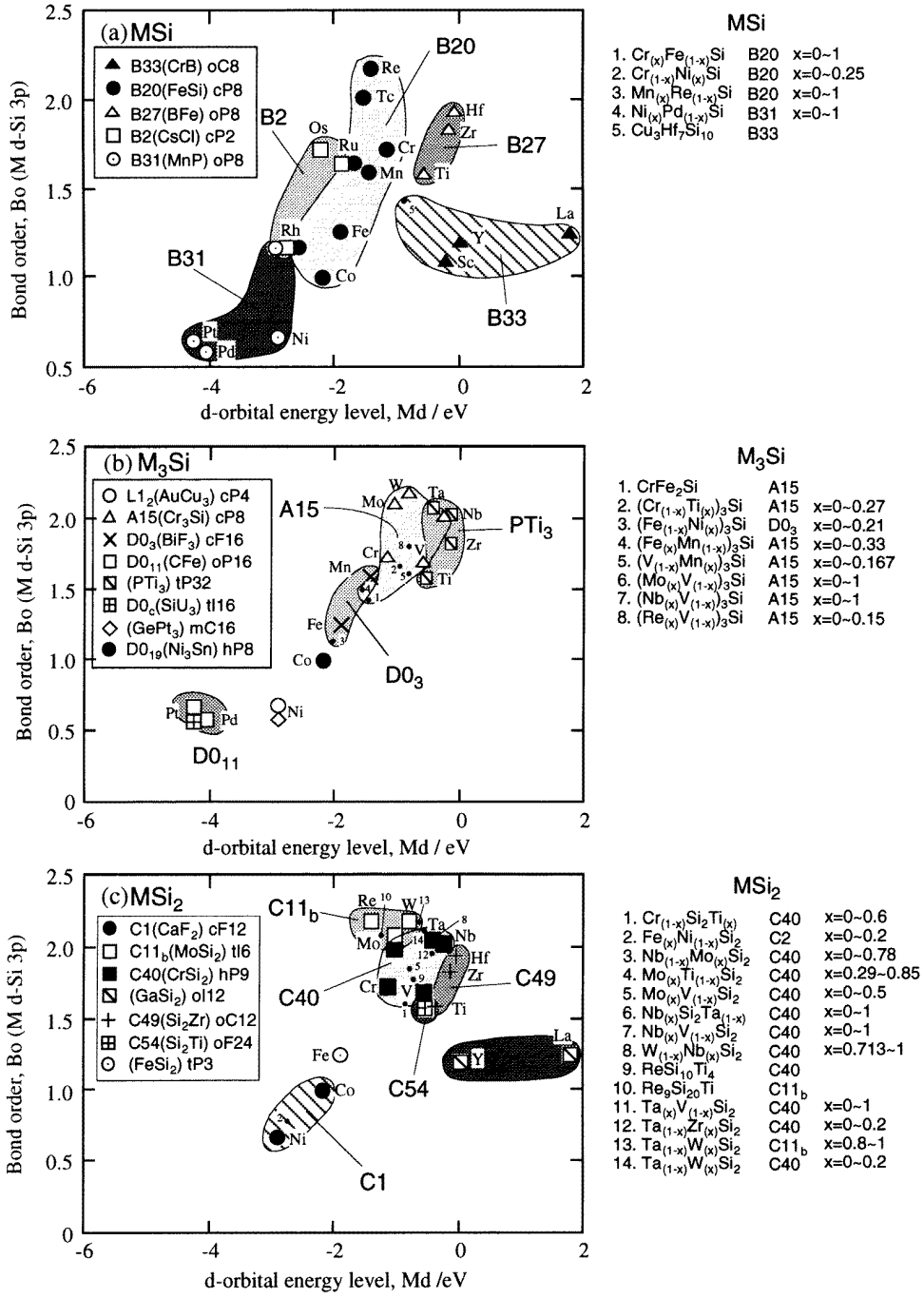

Figure 7. Structure maps for (a) MSi, (b) M_3Si, and (c) MSi_2 compounds.

calculations. As explained before, for crystalline solids, tetrahedron, octahedron, and hexahedron may be important structural units. In fact, as shown in figure 10(a), there are

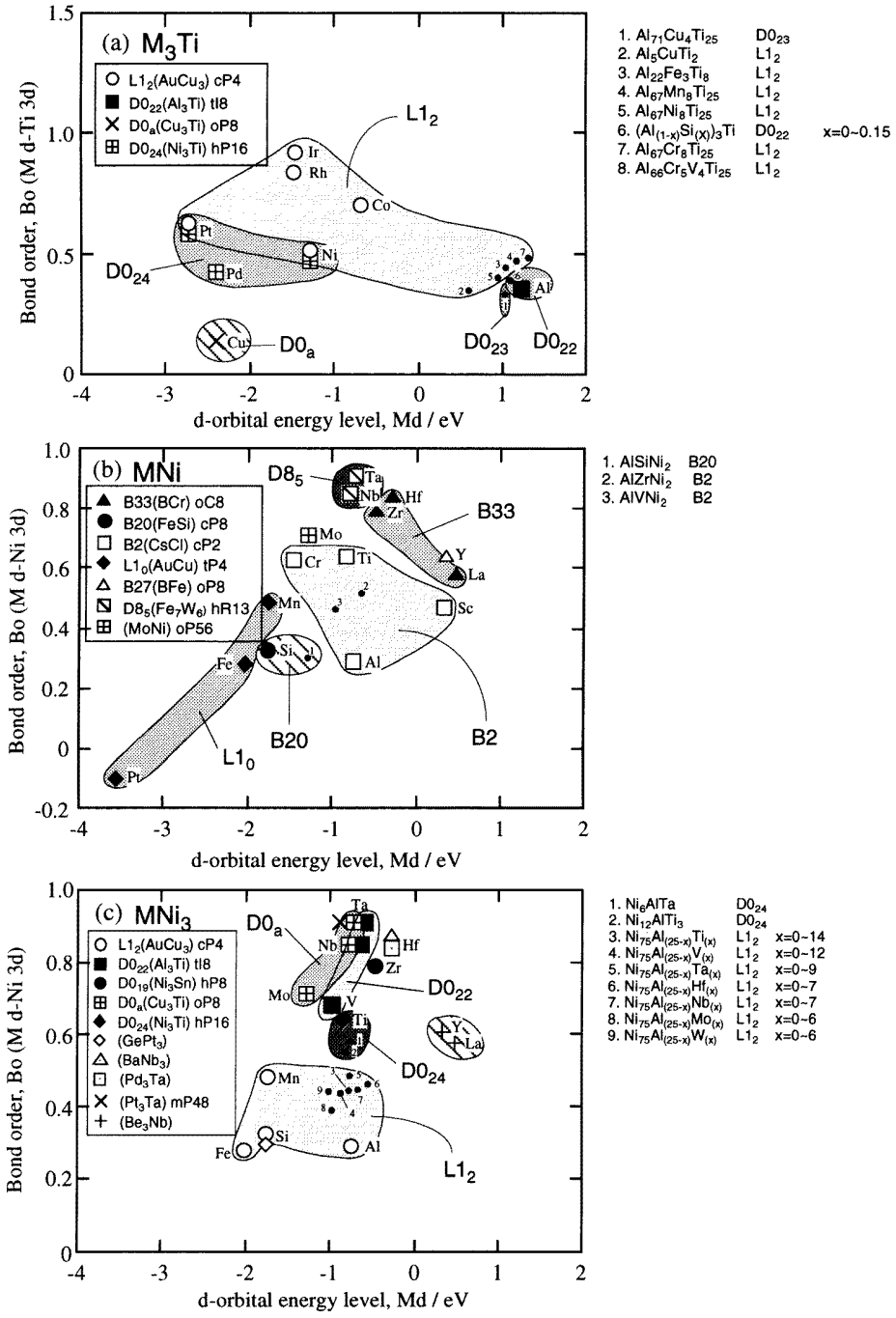

Figure 8. Structure maps for (a) M_3Ti, (b) MNi, and (c) MNi_3 compounds.

all these polyhedra in the $C11_b$-type structure of $MoSi_2$ [1], even though each polyhedron is slightly distorted from the perfect one because of the tetragonal symmetry of the unit cell. Therefore in order to show the validity of the structure maps derived from the calculations

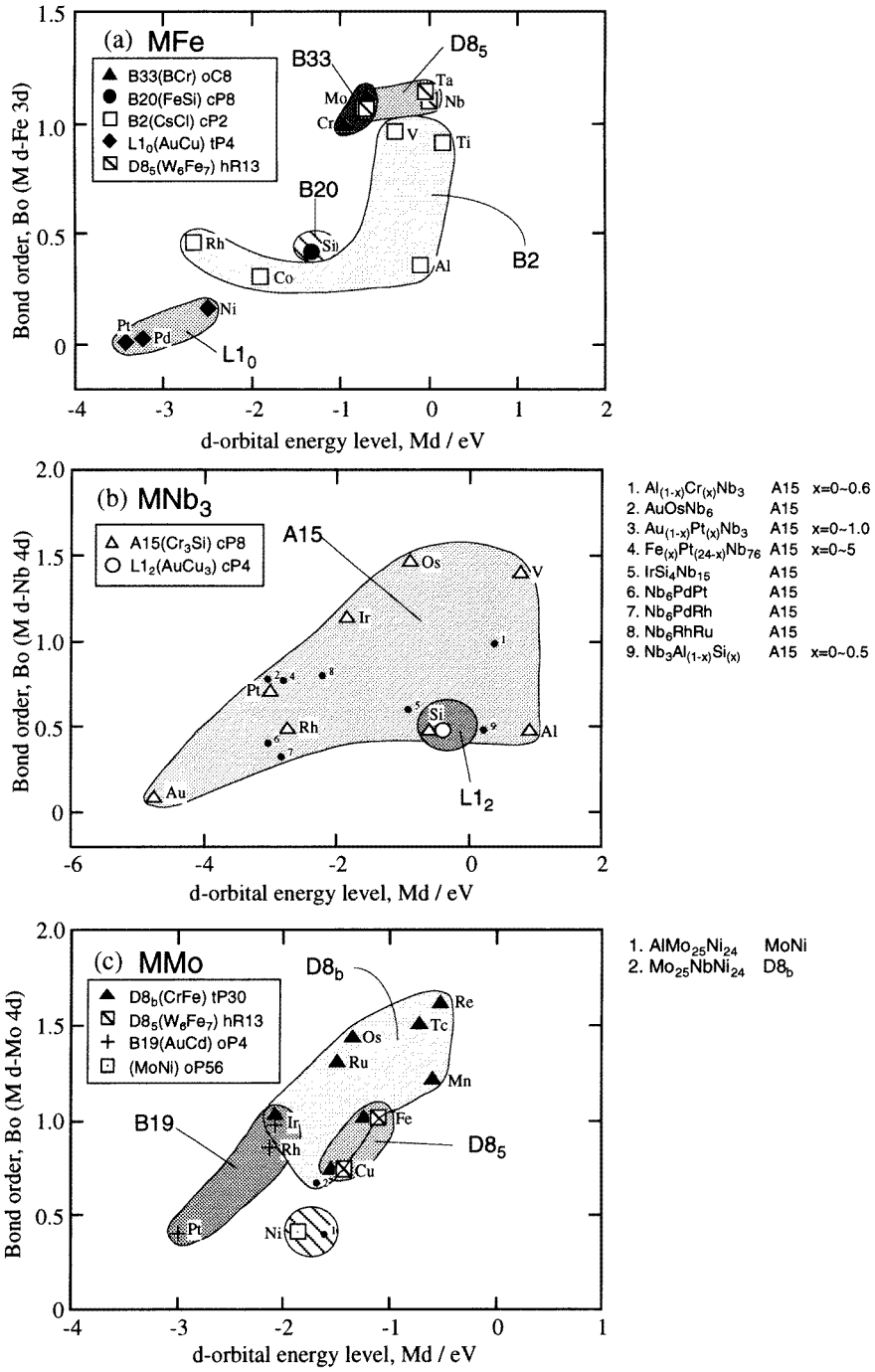

Figure 9. Structure maps for (a) MFe, (b) MNb_3, and (c) MMo compounds.

using an octahedral cluster, further calculation is performed using a $MoSi_2$ cluster model containing three types of polyhedron in it.

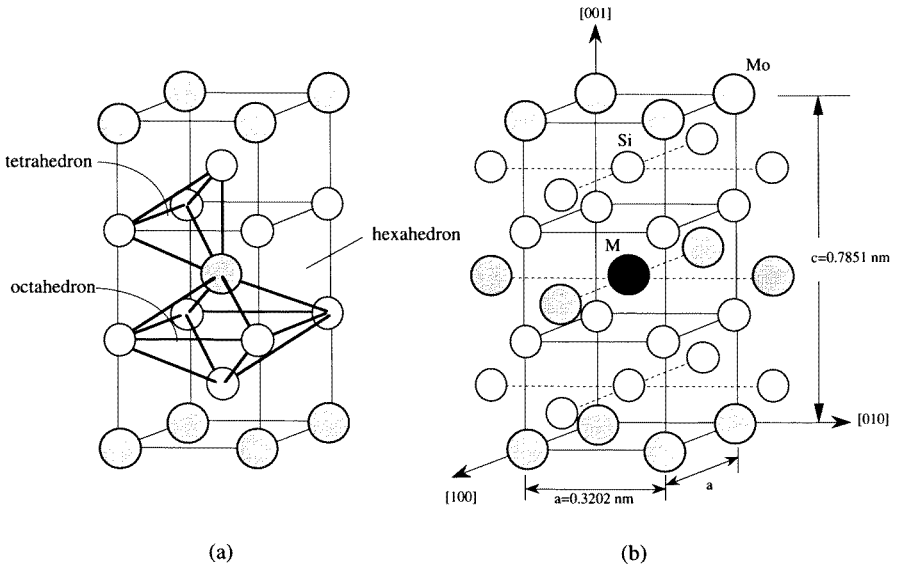

Figure 10. (a) The crystal structure of $MoSi_2$ and (b) the cluster model, $MMo_{12}Si_{18}$, used in the calculation.

5.1. Bo and Md parameters for $MoSi_2$ cluster

The cluster model used for the present calculation is shown in figure 10(b) [23]. In this $MMo_{12}Si_{18}$ cluster, there are four more Mo atoms and eight more Si atoms besides the atoms existing in the unit cell shown in figure 10(a). A series of elements, M, is substituted for the Mo atom at the centre of the cluster, where the M are Ti, V, Cr, Mn, Fe, Co, and Ni (3d transition metals), Zr, Nb, Mo, and Ru (4d transition metals), and Hf, Ta, W, and Re (5d transition metals). The lattice parameters used are $a = 0.3202$ nm and $c = 0.7851$ nm, the same values as in the bulk [1].

The values of Bo and Md are calculated and the detailed derivation of these parameters are given elsewhere [23]. As shown in figure 11(a), the Md parameter changes monotonically with the order of elements in the periodic table. Also, as shown in figure 11(b), the calculated bond orders between Si 3p and M d electrons change periodically following the position of elements in the periodic table. This trend resembles the results of the octahedral cluster shown in figures 5 and 11(a).

5.2. Structure map of disilicides

A structure map is constructed employing the Bo and the Md parameters for a large-cluster model of $MoSi_2$. The results for disilicides are shown in figure 12, and compared with the results shown in figure 7(c) for an octahedral cluster model. Here, for comparison, the individual Bo and Md values are shifted by a certain amount so that the location of $MoSi_2$, namely the position of Mo on the map coincides with the result shown in figure 7(c).

As shown in figure 12, the $MoSi_2$ compound of the $C11_b$-type structure is located in a high-Bo region on this map. Therefore, it may be said that this compound has a stronger chemical bond than other compounds, which causes the higher melting temperature, 2303 K [19]. Also, there is the C40-type region near the $C11_b$-type region. Therefore, the structural

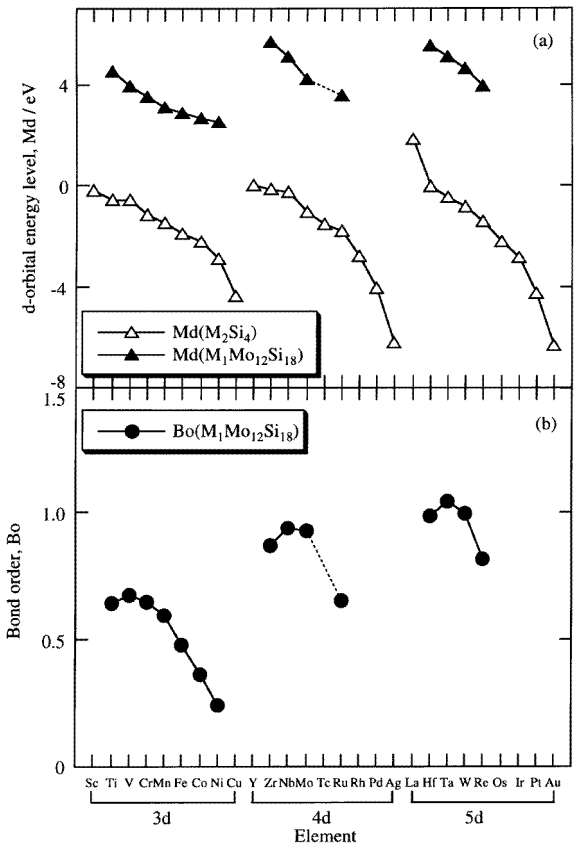

Figure 11. The change in (a) the d-orbital energy level and (b) the bond order with M for $MMo_{12}Si_{18}$ cluster.

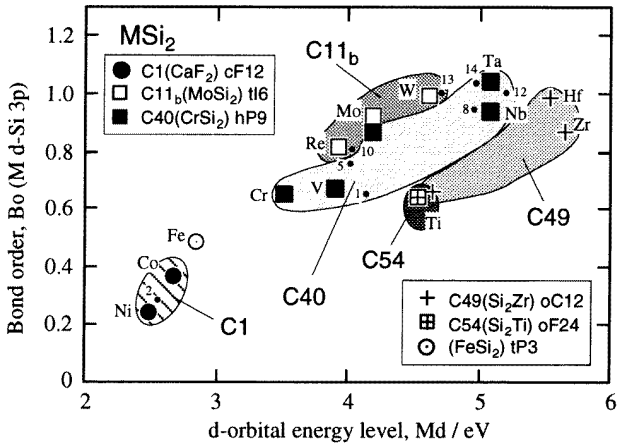

MSi_2

1. $Cr_{(1-x)}Si_2Ti_{(x)}$	C40	x=0~0.6
2. $Fe_{(x)}Ni_{(1-x)}Si_2$	C2	x=0~0.2
3. $Nb_{(1-x)}Mo_{(x)}Si_2$	C40	x=0~0.78
4. $Mo_{(x)}Ti_{(1-x)}Si_2$	C40	x=0.29~0.85
5. $Mo_{(x)}V_{(1-x)}Si_2$	C40	x=0~0.5
6. $Nb_{(x)}Si_2Ta_{(1-x)}$	C40	x=0~1
7. $Nb_{(x)}V_{(1-x)}Si_2$	C40	x=0~1
8. $W_{(1-x)}Nb_{(x)}Si_2$	C40	x=0.713~1
9. $ReSi_{10}Ti_4$	C40	
10. $Re_9Si_{20}Ti$	$C11_b$	
11. $Ta_{(x)}V_{(1-x)}Si_2$	C40	x=0~1
12. $Ta_{(1-x)}Zr_{(x)}Si_2$	C40	x=0~0.2
13. $Ta_{(1-x)}W_{(x)}Si_2$	$C11_b$	x=0.8~1
14. $Ta_{(1-x)}W_{(x)}Si_2$	C40	x=0~0.2

Figure 12. Structure map for MSi_2 compounds obtained from the calculation of $MMo_{12}Si_{18}$ cluster.

modification to the C40 type is possible by adding those elements into $MoSi_2$ (e.g., Cr, Nb, Ta) which form the C40-type compounds, as is confirmed experimentally [3, 24]. The C49-type region seems to extend to the C54-type region of $TiSi_2$, since the C49-type structure is observed in some cases in $TiSi_2$ [25]. Also, both the C1-type region and the C49-type region are located far away from the $C11_b$-type region. Therefore, continuous structural modification from the $C11_b$ type to the C49 type or the C1 type may be impossible by alloying [3]. Not only the structural separation, but also solid solubilities of elements in $MoSi_2$ can be understood with the aid of this Bo–Md map [23]. Therefore, this structure map shown in figure 12 is supposed to be highly reliable.

The structure map shown in figure 7(c) resembles the map shown in figure 12 as a whole. This means that the general trend of the chemical bond between M and X atoms is reproduced well, despite the use of the small-octahedral-cluster model in the calculation. In other words, the Bo and Md parameters obtained from the octahedral cluster will be available for constructing structure maps of the compounds.

6. Comparison with other structure maps

6.1. Miedema's electronegativity and electron density at the Wigner–Seitz atomic cell boundary

Miedema has proposed two parameters to estimate the heat of formation of intermetallic compounds [5]. One is the electronegativity, ϕ^*, and the other is the electron density at the boundary of the Wigner–Seitz atomic cell, n_{ws}. The structure map for M_3Al is constructed using these parameters and the result is shown in figure 13(a). The regions of the $D0_{19}$-type, the $L2_1$-type, the $D0_3$-type, and the $L1_2$-type structures are mixed together on the map. It is evident that this map shows a poorer separation of crystal structures, as compared to the map shown in figure 6(b).

6.2. Zunger's pseudopotential radius

Zunger has calculated the pseudopotential radii of s electrons, r_s, and also of p electrons, r_p. Using these r_s and r_p, dual parameters are obtained for the AB compound as

$$R_\sigma^{AB} = |(r_s^A + r_p^A) + (r_s^B + r_p^B)| \tag{5}$$

$$R_\pi^{AB} = |(r_s^A - r_p^A) + (r_s^B - r_p^B)|. \tag{6}$$

The structure map for MAl made up of these parameters is shown in figure 13(b). The B2-type region is very broad and it is overlapped with both the B20-type and the B33-type regions. Thus, the separation of the crystal structure seems poorer in this map than the map shown in figure 6(a).

6.3. The Mendeleev number

Recently, Pettifor has proposed the usefulness of the Mendeleev number for the structural classification of intermetallic compounds [8, 9]. The magnitude of the Mendeleev number for each element changes as if it forms a one-dimensional chain lying on the periodic table. For the binary A_mB_n compound, the structure map is constructed using two Mendeleev numbers (M_A, M_B). For example, the AB_3 structure map is shown in figure 14 for aluminides and silicides containing transition metals. However, the accuracy of prediction is still poor in this case. For example, as shown in figure 14, either the $L1_2$-type or the $D0_{19}$-type

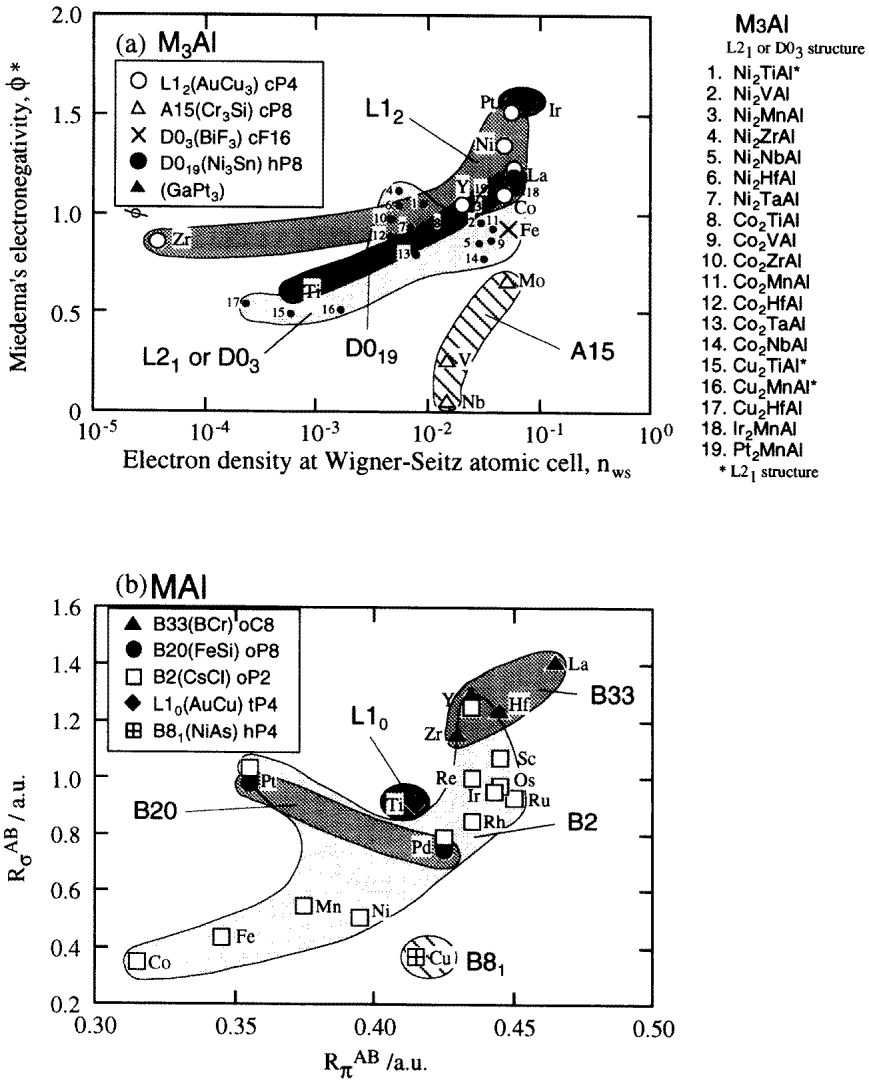

Figure 13. Structure maps for (a) M_3Al compounds with the Miedema parameters and (b) MAl compounds with the Zunger parameters.

region is separated into two different regions on the map. In addition, in this approach the compositional average of the Mendeleev number is taken for the structural classification of pseudo-binary $(A_xX_{1-x})_m(B_yY_{1-y})_n$ systems. Namely, $M_A = x(M_A) + (1-x)(M_X)$, $M_B = y(M_B) + (1-y)(M_Y)$. However, there is a contradiction in some ternary systems. For example, ternary Pt_2MnAl has the $D0_3$-type structure, but this is located in the $L1_2$-type region on the map. The main reason for these discrepancies is probably the lack of two-dimensional periodicity in the single Mendeleev parameter, despite the fact that any compounds having the same crystal structure tend to appear in the same group or near the group in the two-dimensional periodic table. In other words, two parameters are needed to represent the characteristics of two-dimensional periodic table.

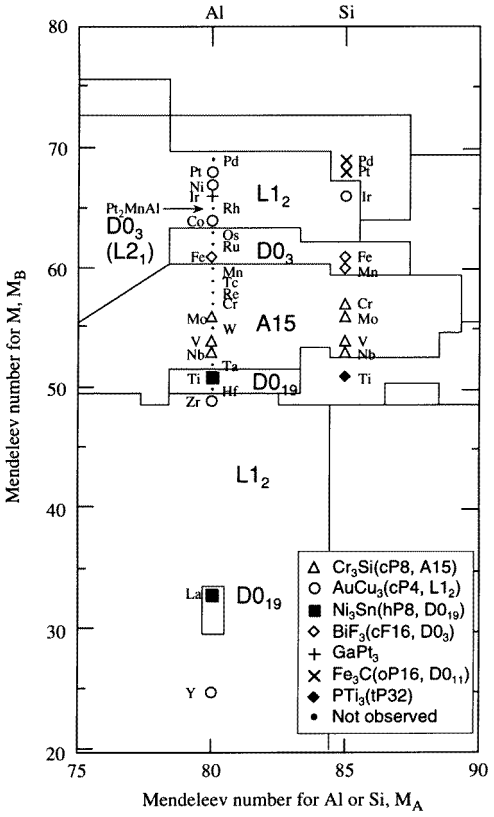

Figure 14. An AB_3 structure map using the Mendeleev number for aluminides and silicides containing transition metals.

On the other hand, there are no such discrepancies on the Bo–Md structure map shown in figure 6(b). For example, Pt_2MnAl of No 19 is positioned in the $D0_3$- (or $L2_1$-) type region, consistent with the experiment. Also, neither the $L1_2$-type region nor the $D0_{19}$-type region ever splits into different regions on this map. Any compounds with the same crystal structure gather together on the map. This is because, as demonstrated in figures 4 and 5, two parameters, Md and Bo, reflect well the nature of the chemical bond between atoms in compounds, while showing a periodical change in the magnitudes, following the order of elements in the two-dimensional periodic table.

7. Structural modification

The possibilities of structural modification by alloying will be discussed with the aid of the present structure maps. Presented here are two examples, Nb_3Al and Al_3Ti. Needless to say, any intermetallic compounds have more than two sublattices in the crystal lattice. When a third element is added into the compound, it is firstly necessary to take into account the substitutional sites of the element. For this reason, special attention is directed toward the substitutional problem in the following discussion.

7.1. The Nb_3Al compound

The Nb_3Al compound having an A15-type crystal structure is one of the promising materials for high-temperature applications, because of its high melting temperature. However, the low ductility at room temperature presents a large barrier to practical use. There may be a possibility of changing the A15-type structure to the more simple $L1_2$-type structure by alloying.

In the M_3Al structure map shown in figure 6(b), the A15-type region is located in a high-Bo region as explained before. This indicates that the A15-type compound has stronger chemical bonding than the $L1_2$-, $D0_{19}$-, $L2_1$-, and $D0_3$-type compounds. Therefore, in order to modify the structure to the $L1_2$-type one, it may be preferable to substitute the lower-Bo elements for Nb atoms. In fact, ternary $NbNi_2Al$ and $NbCo_2Al$ compounds have the $L2_1$-type structure [1]. However, for this modification it is needed to add a large amount of alloying elements into the mother compound. In contrast, Zr_3Al having the $L1_2$-type structure is located just below the A15-type region. Also, the Nb–Zr binary phase diagram shows an all-proportional solid solution at high temperatures without forming any intermetallic compounds. This implies that Zr atoms are substitutable for Nb atoms. The Zr substitution may induce the formation of the $L1_2$-type phase, even though it is not certain whether the microstructure consists of the $L1_2$-type phase alone or two phases of the $L1_2$-type and the A15-type coexisting in the alloy.

On the other hand, in the MNb_3 structure map shown in figure 9(b), there are many A15-type compounds, but the $L1_2$-type compound is limited only to Nb_3Si. Also, as the ternary compound, $Nb_3Al_{(1-x)}Si_x$ ($x = 0$–0.5), keeps the A15-type structure, structural modification of Nb_3Al when third elements are substituted for Al atoms is supposed to be difficult.

7.2. The Al_3Ti compound

Recently, Al_3Ti compound has been received with great interest, because of the low density and excellent oxidation resistance. However, this compound is very brittle at room temperature, partially due to the complexity of the $D0_{22}$-type structure. Recently, there has been an attempt to modify its crystal structure to the $L1_2$ type [2].

For the structure map shown in figure 6(c), the Al_3Ti compound is positioned in a lower-Bo part of the $D0_{22}$-type region. Both the $D0_{19}$-type and the $L1_2$-type regions extend just below the position of Al_3Ti. Therefore, the substitution of the lower-Bo elements for Ti atoms may be able to modify the crystal structure, although there has been no previous report that the $D0_{22}$-type structure is transformed into the $L1_2$-type or the $D0_{19}$-type structure by alloying.

For the M_3Ti structure map shown in figure 8(a), the Al_3Ti compound is located in the highest-Md region among a variety of M_3Ti compounds. The $L1_2$-type region extends over a lower-Md part than the $D0_{22}$-type region. Therefore, it is considered that the substitution of the lower-Md elements for Al atoms is beneficial to the structural modification. In fact, it is known that the $D0_{22}$-type structure is modified to the $L1_2$-type one by the addition of V, Cr, Mn, Fe, Ni, and Cu into Al_3Ti [1, 2].

8. Conclusion

Two electronic parameters, Md and Bo, have been determined by the DV-X_α molecular orbital calculation, and new crystal structure maps have been constructed using these

parameters. It is shown that there is a better separation of the crystal structures for a variety of compounds on these maps, compared to the previously proposed maps. These structure maps are applicable to the prediction of crystal structures not only for binary compounds but also for ternary compounds. Therefore, they are useful for getting an indication of the structural modification by alloying.

Acknowledgments

The authors acknowledge the Computer Centre, the Institute for Molecular Science, Okazaki National Institutes, for the use of the NEC SX-3 model 34R super-computer. This research is supported in part by a Grant-in-Aid for Scientific Research from the Ministry of Education, Science, Sports, and Culture of Japan.

References

[1] Villars P and Calvert L D 1985 *Pearson's Handbook of Crystallographic Data for Intermetallic Phases* vols 1–3 (Metal Park, OH: ASM)
[2] Mabuchi H, Hirukawa K and Nakayama Y 1989 *Scr. Metall.* **23** 1761
[3] Harada Y, Funato Y, Morinaga M, Ito A and Sugita Y 1994 *J. Japan. Inst. Met.* **58** 1239
[4] Massalski T B 1985 *Metall. Trans.* A **20** 1295
[5] Miedema A E 1973 *J. Less-Common Met.* **32** 6439
[6] Zunger A 1980 *Phys. Rev.* B **22** 5839
[7] Villars P 1983 *J. Less-Common Met.* **92** 215
Villars P 1984 *J. Less-Common Met.* **99** 33
Villars P 1984 *J. Less-Common Met.* **102** 199
[8] Pettifor D G 1986 *J. Phys. C: Solid State Phys.* **19** 285
[9] Pettifor D G 1990 *High Temperature Aluminides and Intermetallics* ed S H Whang *et al* Minerals and Materials Society pp 3–17
[10] Adachi H, Tsukada M and Satoko C 1978 *J. Phys. Soc. Japan* **45** 874
[11] Morinaga M, Yukawa N and Adachi H 1985 *Tetsu-to-Hagane* **71** 1441
[12] Morinaga M, Yukawa N and Adachi H 1985 *J. Phys. F: Met. Phys.* **15** 1071
[13] Morinaga M, Yukawa N, Adachi H and Mura Y 1987 *J. Phys. F: Met. Phys.* **17** 2147
[14] Slater J C 1974 *Quatum Theory of Molecules and Solids* vol 4 (New York: McGraw-Hill)
[15] Averill F W and Ellis D E 1973 *J. Chem. Phys.* **59** 6413
[16] Wenninger M J 1971 *Polyhedron Models* (Cambridge: Cambridge University Press)
[17] Mulliken R S 1955 *J. Chem. Phys.* **23** 1833
Mulliken R S 1955 *J. Chem. Phys.* **23** 1841
Mulliken R S 1955 *J. Chem. Phys.* **23** 2338
Mulliken R S 1955 *J. Chem. Phys.* **23** 2343
[18] Hackenbracht D and Kübler J 1980 *J. Phys. F: Met. Phys.* **10** 427
[19] Teatum E T, Gshneidner K A Jr and Waber J T 1968 *Department of Commerce* LA-2345
[20] Watson R E and Bennet L H 1978 *Phys. Rev.* B **18** 6439
[21] Berztiss D A, Cerchiara R R, Gulbransen E A, Pettit F S and Meier G H 1992 *Mater. Sci. Eng.* A **155** 165
[22] Svechnikov V N, Kocherzhinskii Y A and Yupko L M 1970 *Dokl. Akad. Nauk Ukr. SSR* A **6** 553
[23] Harada Y, Morinaga M, Ito A and Sugita Y 1996 *J. Alloys Compounds* **236** 92
[24] Boettinger W J 1992 *Mater. Sci. Eng.* A **155** 33
[25] Beyers R, Coulman D and Merchant P 1987 *J. Appl. Phys.* **61** 5110